

Numerical simulation of branched polymer melts in transient complex flow using pom-pom models

P. Wapperom¹ R. Keunings

*CESAME, Division of Applied Mechanics,
Université catholique de Louvain,
B-1348 Louvain-la-Neuve, Belgium*

Abstract

In recent years, a number of constitutive equations have been derived from reptation theory to describe the rheology of both linear and branched polymer melts. While their predictions in rheometrical flows have been discussed in detail, not much is known of their behaviour in complex flows. In the present paper, we study by way of numerical simulation the transient, start-up flow of branched polymers through a planar contraction/expansion geometry. The constitutive equation is the so-called pom-pom model introduced by McLeish and Larson [1], and later modified by Blackwell *et al.* [2]. By combining the Backward-tracking Lagrangian Particle [3] and Deformation Field [4] methods, we obtain results for the original, integral pom-pom model which makes use of the Doi–Edwards orientation tensor. Two simplified versions of the pom-pom model are also considered, namely one based on the Currie approximation for the orientation tensor, and a differential constitutive equation proposed in [1]. Finally, the simulation results are compared to those obtained with the so-called MGI model proposed recently by Marrucci *et al.* [5] for describing linear polymer melts.

Key words: pom-pom integral and differential models; MGI model; contraction/expansion flow; branched polymers; numerical simulation

¹ Current address: Department of Chemical Engineering, University of Delaware, Newark, Delaware 19713, USA

1 Introduction

Since Doi and Edwards [6] introduced the tube model to describe the rheology of entangled polymer melts and concentrated solutions, much progress has been made on the modelling of both linear and branched polymers. The excessive shear thinning in fast shearing flows present in the basic Doi–Edwards model has recently been alleviated for both type of polymers, though in a very different manner. For branched polymers, on which we focus in this paper, a separate relaxation mechanism for the orientation and stretch of the polymer molecules has been introduced by McLeish and Larson [1]. Using a single-mode model, this allowed to qualitatively predict the behaviour in both shear and elongation of a low-density polyethylene melt. The resulting pom-pom model is of integral type and includes the Doi–Edwards orientation tensor, i.e. it involves statistical averages over tube segments. This rather elaborate orientation tensor is usually replaced by a simpler version when rheometrical results are calculated. It is replaced in [1] by the Currie approximation [7], which does not include CPU time intensive statistical averages, while the independent alignment approximation is used in [8].

As a further simplification, and to facilitate numerical computation in complex flow geometries, an approximate differential equation is proposed in [1]. Differential equations are numerically less demanding, both in memory requirements and computation time. It is on the differential version of the pom-pom model that subsequent papers have focused. Bishko *et al.* [9] performed numerical simulations of contraction flows with the one-mode differential approximation, showing qualitative agreement with experimental data. However, a considerable solvent viscosity was included in the total stress, which masks possible stability problems with the differential pom-pom model. Inkson *et al.* [10] have shown that a quantitative fit can be obtained over a wide range of strain rates for both the shear and extensional viscosities of various branched low-density polyethylenes by introducing multiple, decoupled, relaxation modes into the differential pom-pom approximation. Recently, the pom-pom model has been further refined by Blackwell *et al.* [2] through the introduction of so-called local branch-point displacement. This allows for a smoother fit of the elongation viscosity, in contrast with the sharp transitions obtained in the previous models.

For comparison, we also consider the MGI model [5] which is developed for monodisperse linear polymer melts. In this model, the introduction of convective constraint release overcomes the excessive shear thinning observed in the original Doi–Edwards model. A further refinement in this model is the introduction of a force balance on the entanglement nodes. This results in a different orientation tensor that better predicts the normal stress ratio in simple shear flow.

The correspondence between the models derived from reptation theory and the related approximate equations is not obvious, particularly in complex flow. Indeed some discrepancies between the integral and differential pom-pom models already exist in rheometrical flow as shown in [8]. Recent numerical developments, however, have produced efficient methods for transient simulations of integral models. This allows for a more complete verification of the approximate equations.

To efficiently simulate time-strain separable integral models, the so-called deformation field method has been introduced by Peters *et al.* [4]. In a subsequent paper, Peters *et al.* [11] have shown that the method can equally well be applied to the elaborate integral equations that are obtained from reptation theory. In [11], the method was applied to the Mead–Larson–Doi model. To perform the simulations at higher Weissenberg numbers, however, it was necessary to add a solvent contribution to the polymeric stress. By incorporating the deformation field method in the framework of Lagrangian particle methods, Wapperom and Keunings [12] were able to perform complex flow simulations with the MGI model without adding a solvent stress contribution. In this manner, a better comparison can be made because the solvent may have a considerable impact at high Weissenberg numbers.

In this paper, we focus on branched polymers which can be described by the pom-pom model. We consider in turn the original model with the Doi–Edwards orientation tensor \mathbf{Q} , the Currie approximation of \mathbf{Q} , and the approximate differential equation proposed by [1]. Besides a brief review of the equations of the various stress models and the numerical method, we discuss the behaviour of a one-mode pom-pom melt in rheometrical and complex flows. To distinguish the behaviour of branched and linear polymers, the MGI model is used for comparison.

2 The pom-pom and MGI models

In the integral pom-pom model derived by McLeish and Larson [1], the polymeric stress tensor \mathbf{T} is related to an orientation tensor \mathbf{S} by the algebraic equation

$$\mathbf{T} = G\lambda^2\mathbf{S}, \quad (1)$$

where G is 15/4 times the plateau modulus G_0 and λ represents the dimensionless backbone stretch given by the evolution equation,

$$\frac{D\lambda}{Dt} = \lambda\boldsymbol{\kappa} : \mathbf{S} - \frac{1}{\tau_s}(\lambda - 1)e^{\nu^*(\lambda-1)}, \quad (2)$$

where $\boldsymbol{\kappa}$ is the transpose of the velocity gradient, τ_s the stretch relaxation time, and ν^* a free parameter of order one. The exponential factor has been introduced by Blackwell *et al.* [2] to remove the sharp transitions in the elongational viscosity that are present in the original equation given in [1]. The original equation can be recovered by taking $\nu^* = 0$.

The orientation tensor \mathbf{S} , which measures the distribution of unit vectors describing the orientation of tube segments, is given by an integral equation of the form

$$\mathbf{S} = \int_{-\infty}^t \mu(t; t') \mathbf{Q}(t; t') dt', \quad (3)$$

where $\mu(t; t')$ is a memory function that weights the contribution of the past deformations represented by \mathbf{Q} . For the pom-pom model, the memory function is equal to the Doi–Edwards memory function which can be calculated analytically,

$$\mu(t; t') = \frac{1}{\tau_b} \exp\left(\frac{-(t - t')}{\tau_b}\right), \quad (4)$$

where τ_b denotes the backbone relaxation time.

The tensor $\mathbf{Q}(t; t')$ denotes an orientation tensor at current time t that measures the average orientation of the tube segments with respect to a reference time t' in the past. For both the pom-pom and the Doi–Edwards model this tensor is given by

$$\mathbf{Q} = \frac{1}{\langle |\mathbf{F} \cdot \mathbf{u}| \rangle} \left\langle \frac{\mathbf{F} \cdot \mathbf{u} \mathbf{F} \cdot \mathbf{u}}{|\mathbf{F} \cdot \mathbf{u}|} \right\rangle, \quad (5)$$

where the unit vector \mathbf{u} represents the orientation of a tube segment and the brackets denote an ensemble average. Note that we take the original Doi–Edwards \mathbf{Q} tensor, i.e. without the independent alignment approximation. The deformation gradient tensor \mathbf{F} in Eq. (5) fulfils the differential equation

$$\frac{D\mathbf{F}}{Dt} = \boldsymbol{\kappa} \cdot \mathbf{F}. \quad (6)$$

The integral pom-pom model used in the calculations of [1] applies the so-called Currie approximation [7] for the Doi–Edwards tensor \mathbf{Q} , wherein the orientation tensor \mathbf{S} is directly related to the Finger strain \mathbf{B} and the Cauchy

strain \mathbf{B}^{-1} by

$$\mathbf{Q} = \frac{4}{3(J-1)}\mathbf{B} - \frac{4}{3(J-1)(I_2+3.25)^{1/2}}\mathbf{B}^{-1}. \quad (7)$$

Here, $J = I_1 + 2(I_2 + 3.25)^{1/2}$ and I_1 and I_2 are the first and second invariants of \mathbf{B} , respectively. The model is completed by an evolution equation for the Finger tensor

$$\frac{D\mathbf{B}}{Dt} = \boldsymbol{\kappa} \cdot \mathbf{B} + \mathbf{B} \cdot \boldsymbol{\kappa}^T. \quad (8)$$

Since integral models are computationally more expensive than differential constitutive equations, a differential approximation of Eqs. (3), (7) has been proposed as well in [1]. The approximation consists of a different orientation tensor \mathbf{S} , which is now obtained from a deformation tensor \mathbf{A} which fulfils an evolution equation,

$$\mathbf{S}_A = \mathbf{A}/\text{tr } \mathbf{A}, \quad (9)$$

$$\frac{D\mathbf{A}}{Dt} = \boldsymbol{\kappa} \cdot \mathbf{A} + \mathbf{A} \cdot \boldsymbol{\kappa}^T - \frac{1}{\tau_b}(\mathbf{A} - \mathbf{I}). \quad (10)$$

Except for the modulus G which now equals $3G_0$, the equations for the stress (1) and stretch (2) remain identical.

For comparison, we also discuss the MGI model which has recently been proposed for monodisperse linear polymer melts [5]. This model does not include tube stretch, so the stress is given by

$$\mathbf{T} = G\mathbf{S}, \quad (11)$$

where $G = 6G_0$. The memory function μ in Eq. (3) now depends on the flow conditions and can be written in integral form as

$$\mu(t; t') = \frac{1}{\tau(t')} \exp\left(-\int_{t'}^t \frac{dt''}{\tau(t'')}\right). \quad (12)$$

The overall relaxation time includes a relaxation time due to reptation and one due to convective constraint release (CCR),

$$\frac{1}{\tau} = \frac{1}{\tau_d} + \frac{\beta}{G} \max(0, \boldsymbol{\kappa} : \mathbf{T}), \quad (13)$$

where β is a numerical coefficient somewhat larger than unity to ensure an ever-increasing shear stress as a function of shear rate. Following [12], CCR is made inactive for a negative stress work. (Otherwise, the relaxation time τ could become negative when the velocity gradient changes sign while the stress remains positive due to a finite relaxation time.) The orientation tensor \mathbf{Q} is obtained from a force balance on the entanglement nodes [5] and depends on the square root of the Finger tensor,

$$\mathbf{Q} = \frac{\sqrt{\mathbf{B}}}{\text{tr} \sqrt{\mathbf{B}}}. \quad (14)$$

Note that for this strain measure no averaging over tube segments is involved, contrary to the Doi–Edwards \mathbf{Q} tensor.

3 Fluid parameters and rheometrical flows

In our simulations, we have used values of the model parameters similar to Bishko *et al.* [9] for a molecule with five arms. The ratio of the relaxation times for the orientation and stretch is $\tau_b/\tau_s = 3.24$. To have a direct comparison with our previous results for the MGI model [12], we have taken $\tau_b = 1$. Henceforth, all times and strain rates are expressed relatively to τ_b (or τ_d in case of the integral MGI model), and stresses are measured relatively to G_0 . The extra parameter $\nu^* = 0.64$ is obtained from an empirical constant $k^* = 0.36$, as suggested in [2]. All parameter values we use are listed in Table 1.

Table 1
Fluid parameters for pom-pom and MGI models.

pom-pom	$G_0 = 1$	$\tau_b = 1$	$\tau_s = 0.308$	$\nu^* = 0.64$
MGI	$G_0 = 1$	$\tau_d = 1$	-	$\beta = 3.8$

For these parameter values, we now discuss the rheometrical predictions of the various models. All results have been obtained with a simplified version of the numerical method that we discuss briefly in section 4.

The two rheometrical properties that mainly determine our results in a planar complex flow are the shear and (planar) elongation viscosities. The steady viscosities are depicted in Fig. 1. Indicated in the shear viscosity plot is the -1 slope, which clearly shows the excessive shear thinning of the pom-pom models at high shear rates, particularly for the differential approximation. Up to $\tau_b\dot{\gamma} \simeq 100$, the curves for the pom-pom integral models resemble the MGI viscosity. At higher shear rates, a stronger shear thinning becomes apparent. The

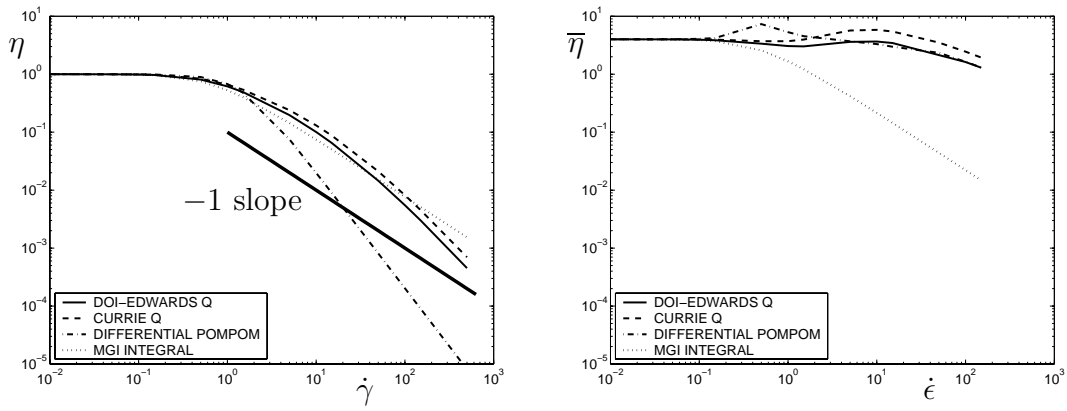


Fig. 1. Shear viscosity η and planar extensional viscosity $\bar{\eta}$ for pom-pom and MGI models.

difference between linear and branched model polymers is clearly seen in the elongational viscosity curves. The pom-pom models show a slight elongational thickening followed by weak thinning. The MGI model, on the other hand, shows extreme elongational thinning, although this is probably too strong due to the lack of tube stretch in that model.

The transient shear viscosity η^+ and planar elongational viscosity $\bar{\eta}^+$ are shown in Fig. 2 for a low, medium, and high deformation rate. As expected, all

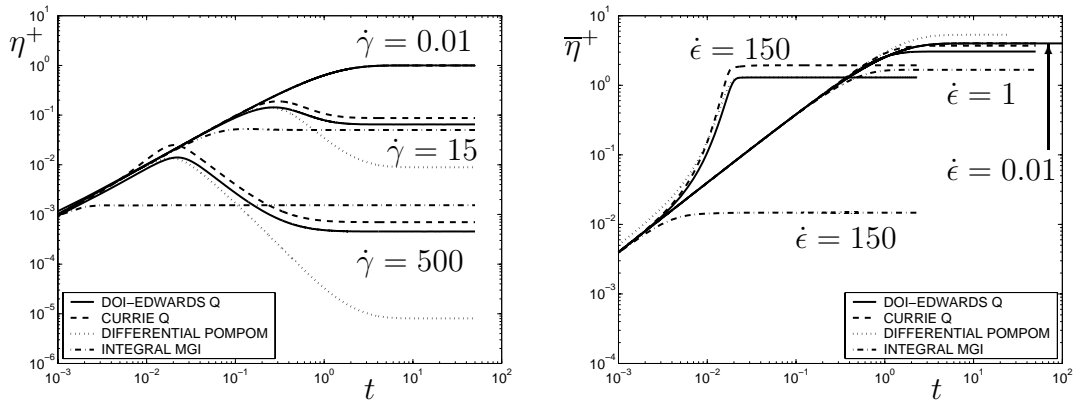


Fig. 2. Transient shear viscosity η^+ and planar elongational viscosity $\bar{\eta}^+$ for pom-pom and MGI models.

models give identical predictions at small strain rates (here $\dot{\gamma}$ or $\dot{\epsilon} = 0.01$). The shear viscosity of the pom-pom models shows an overshoot at higher shear rates, which is absent with the MGI model. The differential approximation is accurate until the maximum viscosity is reached, but after the overshoot the correspondence is very poor. This has also been observed in [8] for different values of the fluid parameters. On the other hand, the correspondence between the various pom-pom models in transient elongational flow is quite good. Here, the contrast with the strongly elongational thinning MGI model is notable. At high elongation rates, the MGI model predicts much lower steady-state values, that are attained much faster and in a smoother manner.

The first and second normal stress coefficients (Fig. 3) look at first sight quite similar for all models, the exception being the differential pom-pom model

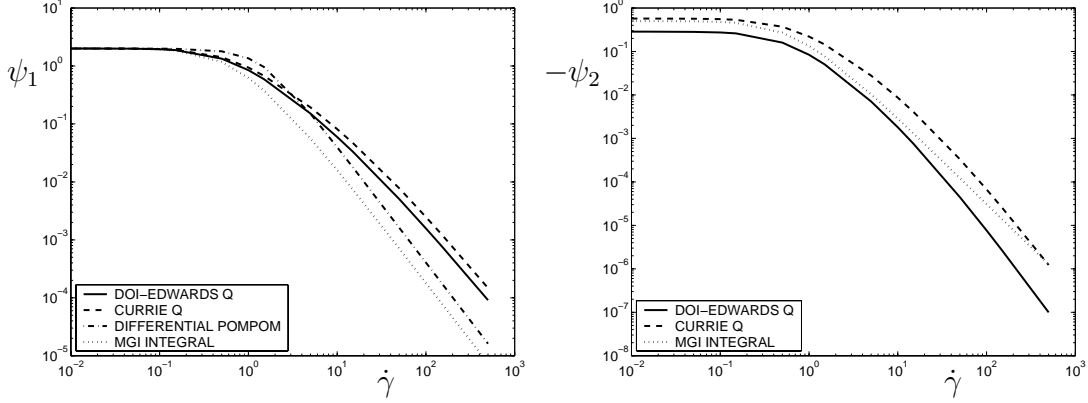


Fig. 3. First and (negative) second normal stress coefficients ψ_1 and $-\psi_2$ for pom-pom and MGI models.

which has a vanishing second normal stress coefficient. The small differences, like the limiting values of ψ_2 at small shear rates and the different asymptotic behaviour at large shear rates, are more apparent in Fig. 4 which shows the ratio of the normal stress differences. At small $\dot{\gamma}$, the original pom-pom model

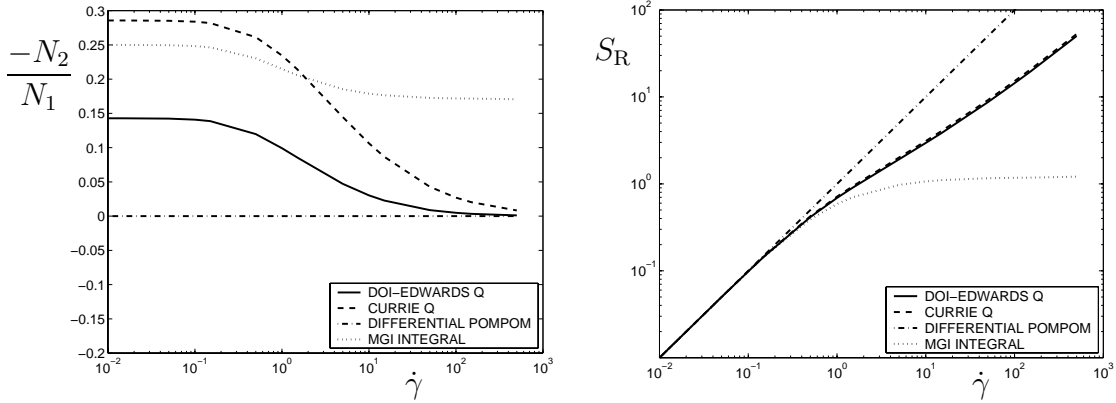


Fig. 4. Normal stress ratio $-N_2/N_1$ and recoverable shear S_R for pom-pom and MGI models.

gives the well-known value of $-N_2/N_1 = -\psi_2/\psi_1 = 1/7$ which is characteristic of the Doi-Edwards \mathbf{Q} tensor. Higher asymptotic values, closer to experimental data, are obtained with the Currie approximation and the MGI model. Also note that, for large strain rates, the pom-pom models give a vanishing stress ratio, while the MGI model predicts a finite positive value.

Also shown in Fig. 4 is the recoverable shear which is a measure of elasticity defined as

$$S_R = \frac{N_1}{2T_{xy}}. \quad (15)$$

Due to the strong shear thinning of the pom-pom models, the recoverable shear grows rapidly. This is particularly true for the extremely shear thinning differential approximation. On the contrary, for the MGI model, S_R only increases slightly at higher shear rates. At $\dot{\gamma} = 500$, the recoverable shear is still as low as 1.21.

4 Governing equations and numerical method

The conservation laws for incompressible, isothermal, and inertialess flow read:

$$\nabla \cdot \mathbf{v} = 0, \tag{16}$$

$$-\nabla p + \nabla \cdot \mathbf{T} = \mathbf{0}, \tag{17}$$

where \mathbf{v} is the fluid velocity, p the hydrodynamic pressure, and the polymeric stress \mathbf{T} is given by either Eq. (1) for the pom-pom models or Eq. (11) for the MGI model. Note that Eq. (17) does not contain any purely viscous component to the stress.

We solve the governing equations by combining the Backward-tracking Lagrangian Particle Method [3] and the method of deformation fields [4]. At each time step, the Eulerian solution of the conservation equations is decoupled from the Lagrangian computation of the polymer stress. In this manner, we can allow for a different solution method well-suited for evolution equations. Since a detailed description of the numerical method can be found in two previous papers [3,12], we only summarise its main characteristics.

The equations of motion (16), (17) are discretised with the aid of the Galerkin finite element method. To increase the stability of the overall numerical scheme, the well-known Discrete Elastic-Viscous Stress Splitting (DEVSS) method [13] has been used.

To compute the integral in Eq. (3) we use the deformation field method as introduced in [4]. A number of N_d deformation fields are introduced that describe the deformation between N_d reference past times and the current time. For the pom-pom models, we define N_d deformation gradient fields when the Doi-Edwards \mathbf{Q} tensor is used, and N_d Finger strain fields in case of the Currie approximation. For the MGI model, we define N_d fields for the Finger strain and the memory function μ . The integral in Eq. (3) can then be approximated by a weighted, finite sum of functions of these fields. In case of the pom-pom model with the Doi-Edwards \mathbf{Q} tensor, the ensemble average in Eq. (5) has to be evaluated. We approximate this average by distributing evenly N_u unit vectors on the surface of the unit sphere at the time of creation, as described by van Heel *et al.* [14]. After accounting for the deformation that

these unit vectors undergo, the \mathbf{Q} tensor is then obtained by replacing the brackets by the average over the obtained N_u tensors $\mathbf{F} \cdot \mathbf{u} \mathbf{F} \cdot \mathbf{u} / |\mathbf{F} \cdot \mathbf{u}|$ and the N_u scalars $|\mathbf{F} \cdot \mathbf{u}|$.

Finally, to solve the approximate differential model or the evolution equation for the deformation tensors and the stretch parameter, we use the Backward-tracking Lagrangian Particle Method (BLPM) described in [3]. In short, we define fixed particle locations at the nodes of quadratic finite elements. Then, for every particle location, we predict at every time step the trajectory of the particle that arrives there by tracking one time step Δt backward in time. At the starting point of the trajectory, we initialise the integrand by interpolation of the nodal point values of a stored finite element field at the corresponding time level $t - \Delta t$. Finally, the ordinary differential equations are integrated along the particle trajectories to obtain the integrand at the fixed particle locations at current time t .

5 Problem description

We consider the start-up flow through a planar 4:1:4 constriction with rounded corners, as depicted in Fig. 5. Around the smallest gap of width H , the con-

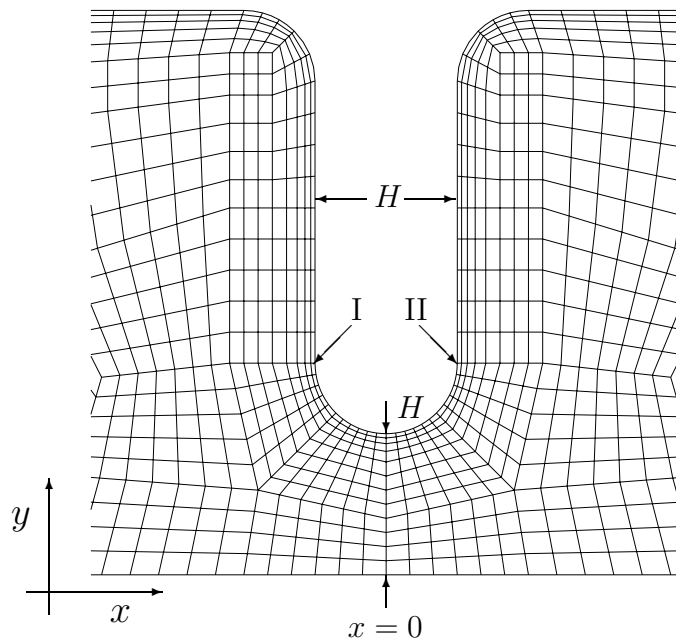


Fig. 5. Zoom of 4:1:4 constriction geometry with rounded corners and medium mesh.

striction wall is circular with diameter H . The lengths of the inlet and outlet regions are taken $19.5H$, and at both inlet and outlet we impose fully developed velocity boundary conditions, which have been calculated separately. No-slip velocity boundary conditions are specified at the wall and symmetry

conditions hold at the centreline. Henceforth, all coordinates are expressed relatively to H .

The results shown below have been obtained with the "medium" mesh used in [12] for the MGI model. That mesh, depicted in Fig. 5, contains 1288 quadrilateral elements and is particularly fine near the constriction wall where steep boundary layers may develop. The smallest element has an area of $\Omega_e = 2.0 \cdot 10^{-3}$. In [12], this mesh was shown to be sufficiently refined for the MGI model. To assure that this mesh is also fine enough for the pom-pom model, we have performed a computation on a finer mesh that has more elements near the constriction wall. In the direction perpendicular to the wall, the smallest element size has been decreased by a factor of two, resulting in a smallest element of $\Omega_e = 8.2 \cdot 10^{-4}$. This finer mesh contains 1352 quadrilateral elements.

In all the simulations, we consider creeping flow, so that, in the absence of a solvent viscosity, the characteristic dimensionless numbers are the Weissenberg numbers for orientation and stretch. Here, we use the orientation Weissenberg number $We = \tau_b U/H$, where U is the average velocity at the smallest gap width H . To evaluate the Doi–Edwards \mathbf{Q} tensor, we have used $N_u = 20$ unit vectors in all simulations presented in this paper. No significant changes were observed with results of a calculation at $We = 3$ with $N_u = 60$. For the DEVSS method, we take the auxiliary viscosity $\eta_{DEVSS} = 6\eta_0 = 6G_0/\tau_b$. As for the computations of the MGI model in [12], this high value was necessary to prevent temporal fluctuations about the steady state regime at high Weissenberg numbers. At low Weissenberg numbers and during start-up of the flow, the results were identical to those obtained with $\eta_{DEVSS} = \eta_0$.

To discretise the memory integral, the past time $t' \leq t$ is divided into 10 intervals with increasing time increments. In all our calculations, we have taken the following number of fields and corresponding time increments: $10 \times \Delta t$, $7 \times 2\Delta t$, $9 \times 4\Delta t$, $10 \times 8\Delta t$, $10 \times 16\Delta t$, $10 \times 32\Delta t$, $10 \times 64\Delta t$, $10 \times 128\Delta t$, $10 \times 256\Delta t$, and $14 \times 512\Delta t$. In previous calculations in [4] and [12] this discretisation has been proven sufficient for obtaining accurate transient results. The total past time spanned by this discretisation is $T = 12.2$, which is larger than the maximum time of 10 after which we stop all calculations. For all simulations, this is sufficient to reach a steady state.

The calculations were performed on a 667 MHz ev67 processor of a DEC Alpha workstation. For the integral pom-pom models, the memory needed to store the $N_d = 100$ deformation fields was 75 MB on the medium mesh. Using $N_u = 20$ to approximate the Doi–Edwards \mathbf{Q} tensor resulted in a CPU time of 5.8 seconds per time step. Increasing the number of tube segments to $N_u = 60$ more than doubled the CPU time to 14 seconds per time step. Using the Currie approximation instead, reduced the CPU time by more than

a factor three to 1.8 seconds per time step. The differential approximation only contains one field instead of the 100 deformation and memory fields, so needing considerably less memory (approximately 1 MB). The CPU time was typically 0.4 seconds per time step. In all cases, we used a constant time step $\Delta t = 10^{-3}$.

6 Results

We first check the mesh convergence of the numerical results for the pom-pom model with the Doi–Edwards \mathbf{Q} tensor. Figure 6 shows the steady-state shear stress and first normal stress difference along the horizontal line drawn through

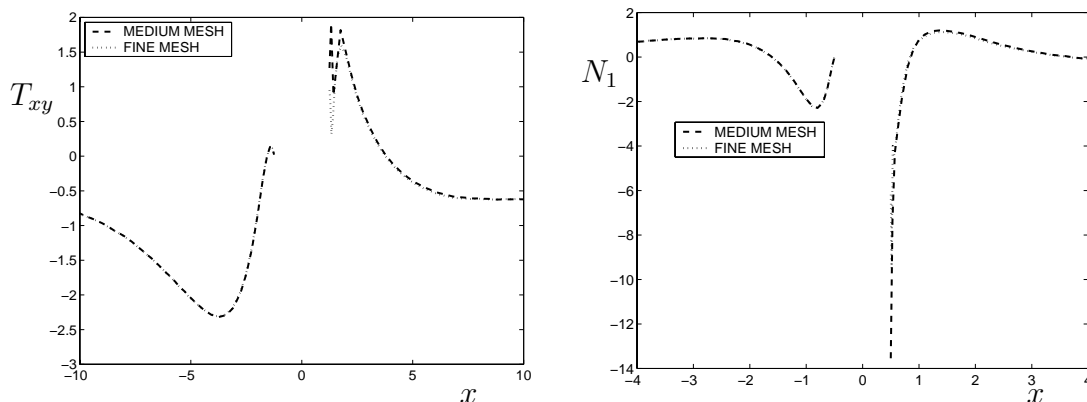


Fig. 6. Mesh convergence for pom-pom model with Doi–Edwards \mathbf{Q} tensor at $We = 10$ near constriction for shear stress T_{xy} and first normal stress difference N_1 along the line $y = 3/2$.

points I and II in Fig. 5. The agreement is excellent, except perhaps in the close vicinity of point II, at the downstream wall. The deviations near this point, however, do not influence the solution elsewhere in the domain. The above mesh convergence behaviour is typical of our simulations with the original pom-pom model, its Currie approximation, and the MGI model. In all cases, a stable steady-state regime was found starting from the rest state. The situation is drastically different for the differential approximation of the pom-pom model. It was indeed found impossible to obtain stable and mesh-converged results with this model, even at small Weissenberg number. (Remember that no purely viscous stress is added.) We believe this is due at least in part to the excessive shear thinning of the differential approximation.

A characteristic and rather sensitive feature of contraction flows is the appearance of vortices. The different rheometrical responses at high Weissenberg number of the pom-pom and MGI models, in particular the behaviour in elongation, result in distinct flow patterns in contraction/expansion flows. In Fig. 7, we display the steady-state streamlines and the vortex intensity. The

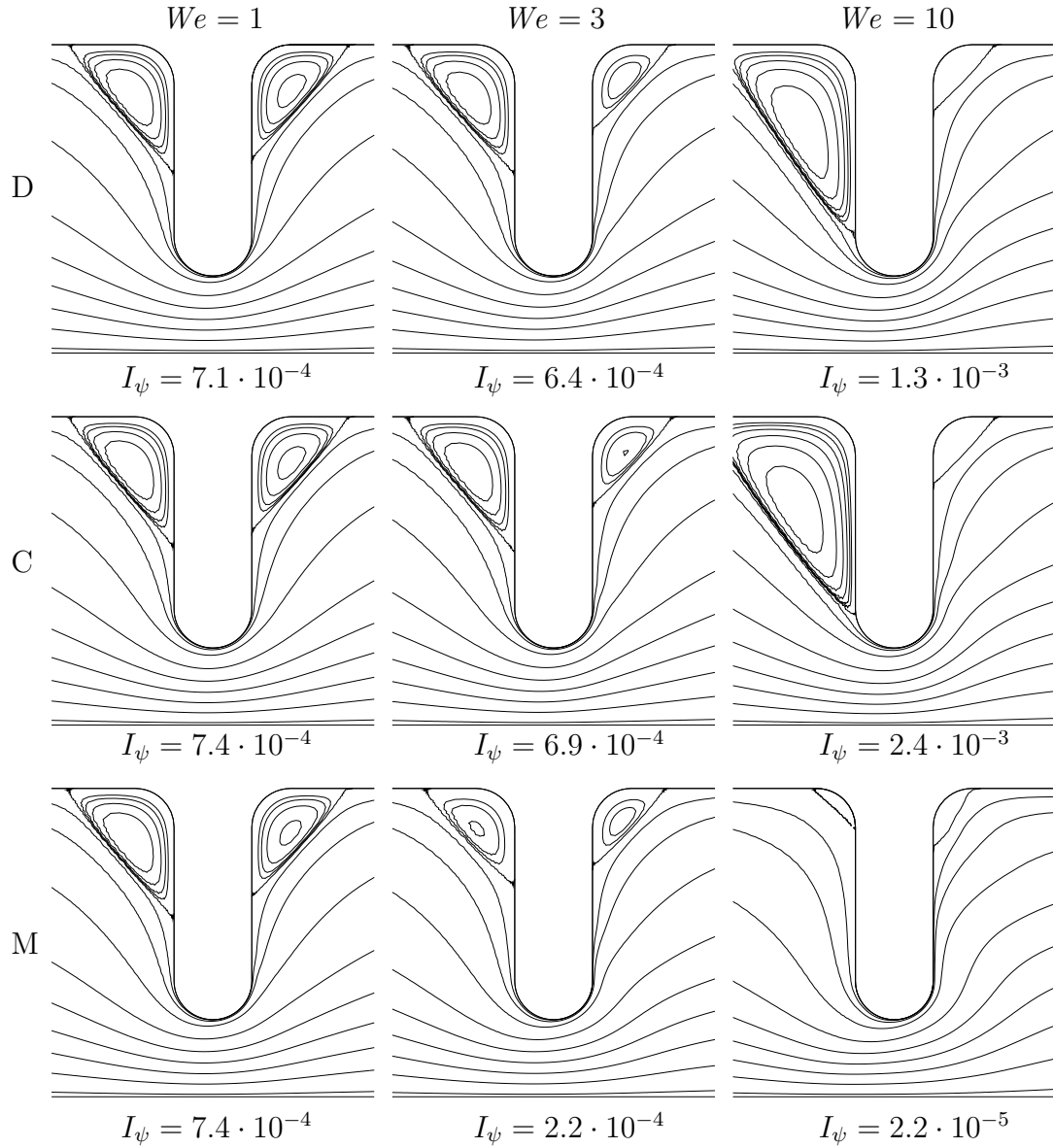


Fig. 7. Steady state streamlines and vortex intensities at various Weissenberg numbers We for pom-pom with Doi–Edwards \mathbf{Q} (D), pom-pom with Currie \mathbf{Q} (C), and integral MGI model (M).

latter is defined as the ratio I_ψ of the amount of fluid flowing in the vortex region and in the main flow. Choosing the zero-value of the stream function at the separating streamline gives

$$I_\psi = -\frac{\psi_{\text{cen}}}{\psi_{\text{ax}}}, \quad (18)$$

where ψ_{cen} and ψ_{ax} denote the values of the stream function at the centre of the vortex and the plane of symmetry, respectively.

For the relatively small Weissenberg number of $We = 1$, i.e. when the rheometrical responses are still very similar except for the normal stress ratio, the flow patterns are practically identical. In fact, we essentially recover the Newtonian limit ($We = 0$) for which the streamlines are symmetrical and $I_\psi = 7.2 \cdot 10^{-3}$. At higher Weissenberg number, the downstream vortex decreases monotonically in a similar fashion for all three models, even though the rheometrical properties of the branched and linear polymers are very different. The upstream vortex, however, behaves very differently. For the MGI model, it decreases in size and intensity similarly to the downstream vortex. For the pom-pom models, however, the vortex intensity decreases slightly for $We = 3$ while the size remains unaltered. At $We = 10$, a substantial increase of both the vortex size and intensity is observed. This is in qualitative agreement with experimental observation for branched polymer melts (see e.g. [15]). The high Weissenberg flow is also the case where the differences between the Doi–Edwards \mathbf{Q} tensor and the Currie approximation become apparent. Both the vortex size and intensity are significantly overpredicted by the latter.

A second important global quantity is the pressure drop. To eliminate the influence of the length of the inlet and outlet regions, we define the pressure drop in the constriction as $\Delta p^c = \Delta p - \Delta p^0$, where Δp is the total pressure drop in the flow and Δp^0 the pressure drop corresponding to a fully developed flow in a channel without the constriction, i.e. of length $40H$ and width $4H$. In Fig. 8, we have non-dimensionalised Δp^c with the pressure drop Δp^0 . Despite their

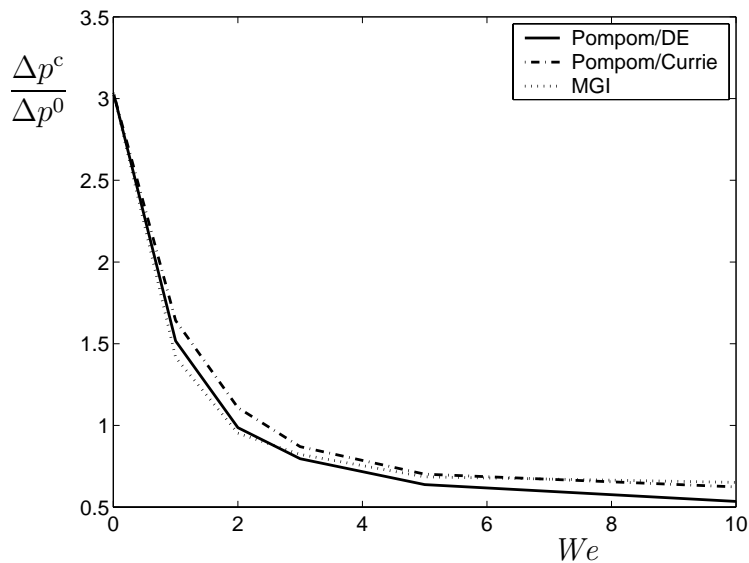


Fig. 8. Non-dimensional pressure drop $\Delta p^c/\Delta p^0$ as a function of Weissenberg number for pom-pom and MGI models.

very different kinematic behaviour, the pom-pom and MGI models predict practically the same pressure drop curve. It would thus seem that the steady-state shear viscosity (Fig. 1) governs the pressure drop in this flow geometry.

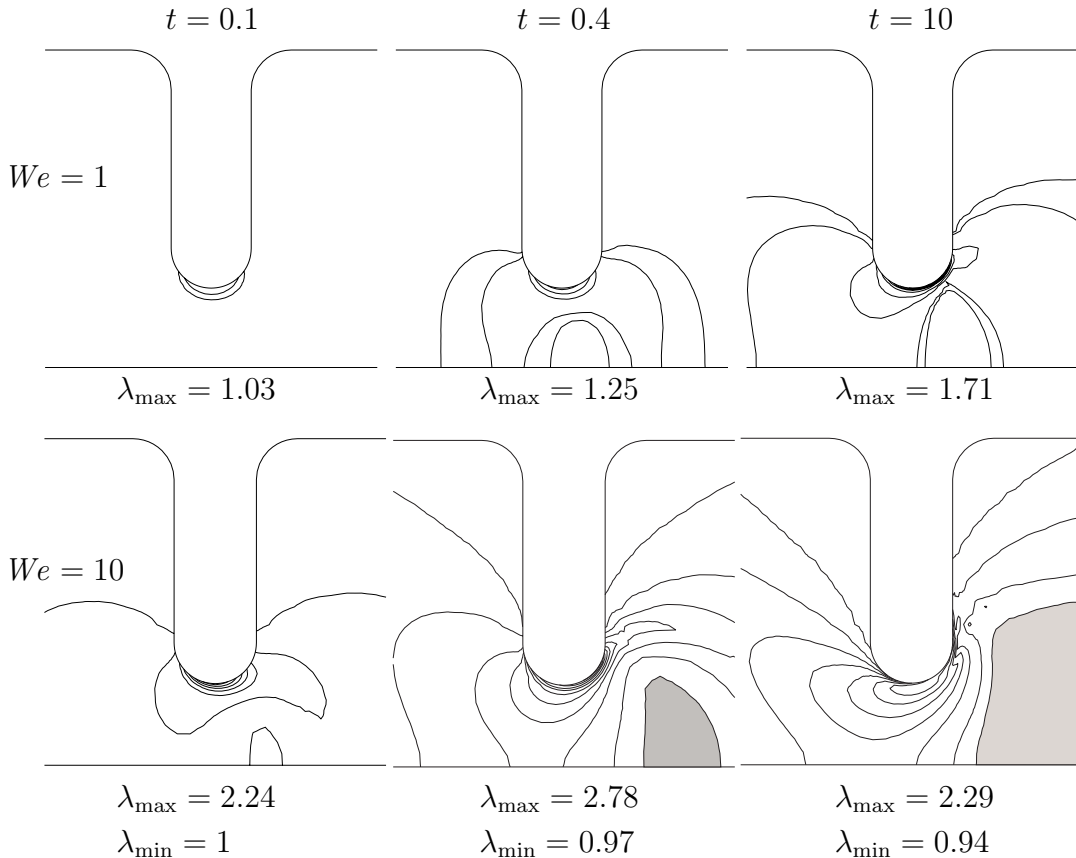


Fig. 9. Time evolution of stretch parameter λ at $We = 1$ and $We = 10$ for pom-pom model with Doi-Edwards \mathbf{Q} . Regions $\lambda < 1$ are shaded. In all cases, λ_{\max} occurs at the constriction wall.

In fact, as shown in [12], a purely-viscous Carreau-Yasuda fit of the MGI shear viscosity yields essentially the same pressure drop curve.

The final quantity we examine here is the stretch parameter λ , which is characteristic of the pom-pom model. The temporal evolution of this parameter is shown in Fig. 9 at $We = 1$ and 10. At low Weissenberg number, the stretch increases monotonically until about $t = 1.6$ where a maximum of 1.75 is reached. The maximum value at steady state is 1.71. At short times, the contour lines are nearly symmetric around $x = 0$, while at steady state the global maximum at the wall and the local maximum at the centreline shift downstream. At high Weissenberg number, elasticity results already at short times in a distinct asymmetry. Furthermore, a clear overshoot in the stretch is obtained, like in simple shear flows [1]. Note that the stretch parameter λ becomes smaller than unity downstream of the constriction. This apparently surprising result can be made plausible by a simple analysis of Eq. (2). Assume that λ reaches

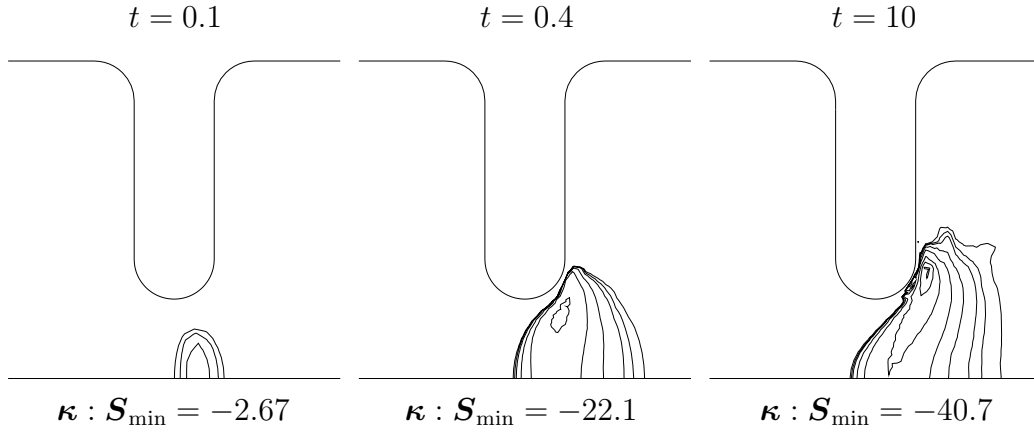


Fig. 10. Time evolution of regions with negative $\kappa : \mathbf{S}$ at Weissenberg number $We = 10$ for pom-pom model with Doi-Edwards \mathbf{Q} .

unity somewhere in the flow field. Then Eq. (2) reduces to

$$\frac{D\lambda}{Dt} = \kappa : \mathbf{S}. \quad (19)$$

Clearly, the further evolution of λ along a fluid trajectory will be such that $D\lambda/Dt < 0$ if $\kappa : \mathbf{S}$ is locally negative. As a result, λ will become smaller than unity. The $\kappa : \mathbf{S}$ is indeed likely to change sign downstream of the constriction, since κ changes sign there quite rapidly along the flow trajectories while the orientation tensor \mathbf{S} needs a finite relaxation process to change sign. Figure 10 displays contour lines for negative values of $\kappa : \mathbf{S}$. It shows that only when the magnitude of the negative $\kappa : \mathbf{S}$ is large enough ($t = 0.4$, $t = 10$), the minimum value of λ falls below one (Fig. 9). Furthermore, due to the finite relaxation time τ_s of the stretch parameter, the region $\lambda < 1$ does not coincide with the region of negative $\kappa : \mathbf{S}$, but is shifted downstream. Except for this shift, the situation is similar to convective constraint release in the MGI model where the overall relaxation time may become negative due to a negative $\kappa : \mathbf{S}$ [12]. This made it necessary to include the maximum in Eq. (13). For the stretch λ , the situation is not as dramatic, because it always remains positive. This can easily be verified by substituting $\lambda = 0$ in the right-hand side of Eq. (2), giving a positive derivative at $\lambda = 0$. However, to avoid the unphysical situation $\lambda < 1$, the $\kappa : \mathbf{S}$ term should be replaced by a strictly positive one.

7 Concluding remarks

We have shown results for transient simulations in complex flow of branched polymer melts using integral pom-pom models. By using the Backward-tracking

Lagrangian Particle Method in combination with the deformation field method, we could obtain stable and mesh-convergent results at high Weissenberg numbers in a contraction/expansion flow without including any purely-viscous "solvent" stress. The original pom-pom model with the Doi–Edwards orientation tensor \mathbf{Q} has been compared with an integral equation employing the Currie approximation for \mathbf{Q} , and with a differential equation based on a configuration tensor.

We found that up to moderate Weissenberg numbers, the Currie \mathbf{Q} tensor is a good approximation of the Doi–Edwards tensor. At higher Weissenberg number, however, the vortex upstream of the contraction/expansion grows considerably faster, both in size and intensity. The differential approximation fails to accurately represent the integral versions of the pom-pom model in fast shearing flows. There it shows an excessive shear thinning, which prevented us from obtaining mesh-converged solutions in complex flow. Comparison with the MGI model for linear polymers, showed a very similar behaviour for the pressure drop and the vortex downstream of the contraction/expansion. Upstream of the contraction, however, a large vortex develops for the pom-pom models while it decreases for the MGI model.

In the complex flow simulations, we also observed an unphysical behaviour for the pom-pom stretch parameter that cannot be observed in steady and start-up rheometrical flows. Indeed, at high Weissenberg number, the stretch may become smaller than unity when $\kappa : \mathbf{S}$ becomes negative, which is physically unrealistic. This happens in flow regions where the velocity gradient changes sign, as for example downstream of a contraction/expansion.

Acknowledgements

This work is supported by the EC TMR contract FMRX-CT98-0210 and the ARC 97/02-210 project, Communauté Française de Belgique.

References

- [1] T.C.B. McLeish and R.G. Larson. Molecular constitutive equations for a class of branched polymers: The pom-pom polymer. *J. Rheology*, 42:81–110, 1998.
- [2] R.J. Blackwell, T.C.B. McLeish, and O.G. Harlen. Molecular drag-strain coupling in branched polymer melts. *J. Rheology*, 44:121–136, 2000.
- [3] P. Wapperom, R. Keunings, and V. Legat. The backward-tracking Lagrangian particle method (BLPM) for transient viscoelastic flows. *J. Non-Newtonian Fluid Mech.*, 91:273–295, 2000.
- [4] E.A.J.F. Peters, M.A. Hulsen, and B.H.A.A. van den Brule. Instationary Eulerian viscoelastic flow simulations using time separable Rivlin–Sawyers constitutive equations. *J. Non-Newtonian Fluid Mech.*, 89:209–228, 2000.
- [5] G. Marrucci, F. Greco, and G. Ianniruberto. Integral and differential constitutive equations for entangled polymers with simple versions of CCR and force balance on entanglements. *Rheol. Acta*, 2000. Submitted.
- [6] M. Doi and S.F. Edwards. *The theory of polymer dynamics*. Clarendon Press, Oxford, 1986.
- [7] P.K. Currie. Constitutive equations for polymer melts predicted by the Doi–Edwards and Curtiss–Bird kinetic theory models. *J. Non-Newtonian Fluid Mech.*, 11:53–68, 1982.
- [8] P. Rubio and M.H. Wagner. LDPE melt rheology and the pom-pom model. *J. Non-Newtonian Fluid Mech.*, 92:245–259, 2000.
- [9] G.B. Bishko, O.G. Harlen, T.C.B. McLeish, and T.M. Nicholson. Numerical simulation of the transient flow of branched polymer melts through a planar contraction using the ‘pom-pom’ model. *J. Non-Newtonian Fluid Mech.*, 82:255–273, 1999.
- [10] N.J. Inkson, T.C.B. McLeish, O.G. Harlen, and D.J. Groves. Predicting low density polyethylene melt rheology in elongational and shear flows with “pom-pom” constitutive equations. *J. Rheology*, 43:873–896, 1999.
- [11] E.A.J.F. Peters, A.P.G. van Heel, M.A. Hulsen, and B.H.A.A. van den Brule. Generalisation of the deformation field method to simulate advanced reptation models in complex flows. *J. Rheology*, 44:811–829, 2000.
- [12] P. Wapperom and R. Keunings. Simulation of linear polymer melts in transient complex flow. *J. Non-Newtonian Fluid Mech.*, 95:67–83, 2000.
- [13] R. Guénette and M. Fortin. A new mixed finite element method for computing viscoelastic flows. *J. Non-Newtonian Fluid Mech.*, 60:27–52, 1995.
- [14] A.P.G. van Heel, M.A. Hulsen, and B.H.A.A. van den Brule. Simulation of the Doi–Edwards model in complex flow. *J. Rheology*, 43:1239–1260, 1999.

- [15] B. Tremblay. Visualisation of the flow of linear low density polyethylene/low density polyethylene blends through sudden contractions. *J. Non-Newtonian Fluid Mech.*, 43:1–29, 1992.